Nonlinear longitudinal waves in a two-dimensional screened Coulomb crystal

S. Nunomura,* S. Zhdanov,† and G. E. Morfill
Max-Planck-Institut für Extraterrestrische Physik, D-85740 Garching, Germany

J. Goree
Department of Physics and Astronomy, The University of Iowa, Iowa City, Iowa 52242, USA
(Received 11 April 2003; published 19 August 2003)

Nonlinear interactions of longitudinal waves were observed in a two-dimensional plasma crystal, i.e., a lattice composed of highly charged microspheres immersed in a plasma. The waves were launched by radiation pressure of a laser, and wave spectra in ω-$\mathbf{k}$ space were analyzed at various amplitudes of waves. At a sufficiently large amplitude of wave, the second and third wave harmonics satisfying a dispersion relation were observed. As the second harmonic propagates from the excitation region, it was amplified for a small distance, and then damped. The experimental results were compared to a nonlinear wave theory and to a molecular dynamic simulation.

DOI: 10.1103/PhysRevE.68.026407 PACS number(s): 52.27.Lw, 52.35.Mw, 52.27.Gr, 82.70.Dd

I. INTRODUCTION

Generation of wave harmonics is one of the prominent features of nonlinear wave-wave interactions in various kinds of matters. To generate wave harmonics from nonlinear wave coupling, it is commonly known that two resonance conditions must be met [1]: $\Sigma\omega_i=0$ and $\Sigma\mathbf{k}_i=0$, where ω_i and $\mathbf{k}_i$ are frequencies and wave numbers of the waves involved in the interaction, respectively. For example, the second (2nd) harmonic is generated by a coupling of the two fundamental modes, and the third (3rd) harmonic is generated by a coupling of the fundamental and second harmonics, or three wave coupling of the fundamental modes in the same manner.

Our system is a two-dimensional (2D) triangular lattice made from a complex plasma, also known as dusty plasma. It contains four components: electrons, ions, microsphere particles, and gas molecules. The particles typically acquire large negative charges by collecting electrons and ions, while the electrons have a higher mobility. The interaction between particles is known to be a screened Coulomb potential [2] because the charges on particles are shielded by surrounding electrons and ions. When these particles are trapped by an external confinement potential and cooled down enough through interactions with the gas molecules, particles form an ordered structure, called a plasma crystal [3–5]. A plasma crystal is an example of a strongly coupled Coulomb system; it is distinguished from some other types of strongly coupled plasmas by the screened Coulomb interaction.

In a 2D plasma crystal, two eigenwave modes can propagate: a longitudinal and a transverse wave. The longitudinal wave is a wave of compression propagating parallel to the particle motion. The transverse wave, sometimes called the shear wave, is a wave propagating perpendicular to the particle motion. In the linear wave regime, i.e., regime where wave amplitude is much smaller than the mean interparticle spacing, both longitudinal and transverse modes have already been observed in several experiments [6–10] and the measured dispersion relations agreed with theoretical predictions [11–13].

Here, we summarize characteristics of wave dispersion relations of longitudinal and transverse modes in 2D plasma crystals, which have been verified in above mentioned experiments and theories. (i) Both modes have acoustic behavior, i.e., $\omega\propto k$ at $k\approx 0$. (ii) The sound speeds of these two modes are different. The longitudinal mode propagates faster than the transverse mode. (iii) Dispersion relations exhibit anisotropy, which is more pronounced in large values of k.

In addition to the longitudinal and transverse waves, which are elastic deformations of the lattice, there are several other modes of particle motion. If the lattice has a finite size, and is confined by an external potential, it will have eigenmodes including the sloshing mode, which is a rigid-body oscillation of the entire lattice in the confining potential. An indirect observation of the presence of the sloshing mode at the same time as a longitudinal wave was reported previously [9].

In addition, a lattice can be deformed with a plastic deformation, i.e., with a breaking of interparticle bonds. When bonds are broken, energy is consumed in an irreversible process, unlike an elastic deformation which involves no breaking of bonds and is reversible in the absence of any friction. A shear in the particle velocity profile is particularly effective in breaking bonds. After bonds have been broken in a plastic deformation process, it is possible for particles to circulate in a vortex, driven by any shear force that might be present. This vortex can be thought of as yet another kind of mode for particle motion. For all these modes, gas friction can lead to a damping.

Nonlinear properties of a longitudinal pulse were recently studied in 2D plasma crystals. Samsonov *et al.* [14] launched a large pulse by applying an electrostatic disturbance to their crystal, and observed what they identified as solitons at larger pulse amplitudes. Nosenko *et al.* [15] also excited a

*Electronic address: nunomura@mpe.mpg.de
†Permanent Address: Moscow State Engineering and Physics Institute, Plasma Physics Department, Kashirskoe 31, 115409 Moscow, Russia.

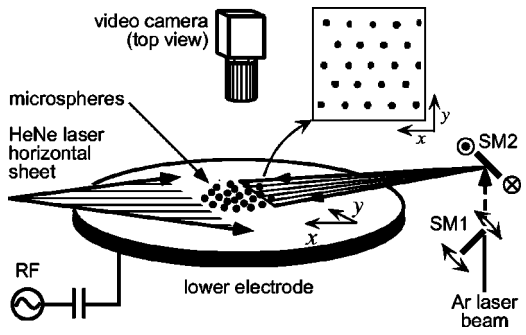

FIG. 1. Sketch of experimental setup. A monolayer plasma crystal was formed in a rf glow discharge. A compressional wave was launched by radiation pressure of an argon laser. The inset is part of the crystal, showing an ordered structure composed of triangular lattice. The *x* and *y* coordinates are shown.

nonlinear pulse, but using a laser manipulation method. They observed that the propagation speed increased with the pulse amplitude. Melzer *et al.* [16] applied a moving disturbance to a lattice, producing a wake composed of longitudinal waves that exhibited a spatial distribution (Mach cone angle). It varied with the intensity of the disturbance; the experiments suggested that this observation might be explained by nonlinear effects. On the theory side, Melandsø [17] investigated nonlinear wave properties in a 1D lattice, and Zhdanov *et al.* [18] recently studied a soliton in 2D triangular lattice.

In this paper, we present experimental results for generation of longitudinal wave harmonics in a 2D plasma crystal. The results are compared to a nonlinear wave theory and to a molecular dynamics (MD) simulation. Then, nonlinear wave-wave interactions are discussed.

II. CRYSTAL FORMATION AND OBSERVATION

Our experiments were performed in a capacitively coupled rf discharge. A sketch of the experimental apparatus is shown in Fig. 1. It is the same experimental device previously used for linear wave experiments [8,9]. By applying 13.56 MHz rf power to the lower electrode through a matching network, an argon plasma was generated at a gas pressure of 15 mtorr. The voltage applied to lower electrode was 88 V peak-to-peak with respect to the grounded vacuum chamber (not shown in Fig. 1). The self-bias voltage appeared on the lower electrode was -44.6 V, which helped to suspend particles in the plasma sheath against gravity. In the bulk plasma, the electron temperature and density were measured with a Langmuir probe, and found to be ≈ 1 eV and 4×10^8 cm^{-3}, respectively. The probe was located in the main plasma, not in the sheath where the particles were levitated.

After the particles were dispersed into the plasma, they were trapped as a monolayer suspension levitated below the bulk plasma, in the plasma sheath above the lower electrode. The particles were confined horizontally by an external potential that was provided naturally by the bowl-shaped curvature of the plasma sheath. The particles arranged themselves in a triangular crystalline lattice, as shown in the inset of Fig. 1. The diameter of the particle suspension was ≈ 7 cm, while the interparticle spacing was measured to be $a=0.9$ mm. The particles were melamine-formaldehyde microspheres with 4.04 μm radius and 1.51 g/cm^3 mass density, corresponding to a particle mass $m=4.17\times 10^{-13}$ kg.

To observe particle motions in the plasma crystal, we illuminated the particles with a He-Ne laser sheet and obtained a top view of the crystal with a conventional video camera. Our viewing area was 24×18 mm^2 of the central region of a crystal, in which approximately 600 particles were included. Using image-processing programs [19], all particle positions were identified and their orbits were traced for several seconds, with a total of 128 frames at 15 frames per second.

III. NATURALLY OCCURRING WAVES AND CRYSTAL PARAMETERS

Like any kinds of solid matters with a finite temperature, in our plasma crystal, particles always exhibited random motions around their equilibrium positions [10]. Particle velocities had a Maxwellian distribution with a width corresponding to the crystal temperature of $T=0.031$ eV, which is slightly higher than the neutral gas temperature 0.025 eV. This higher temperature indicates that particles in our plasma crystal were heated by a surrounding plasma. As a possible candidate for this, we could consider stochastic charge and electric field fluctuations, which give energy to particles [20].

We analyzed correlations among random particle motions to extract self-ordered motions that occur naturally, i.e., to detect naturally occurring waves (natural phonons). Figure 2(a) shows an energy density spectrum of naturally occurring longitudinal waves in ω-$\mathbf{k}$ space. Wave energies $E_{\omega,\mathbf{k}}$ are concentrated only in certain areas, not distributed all over the ω-$\mathbf{k}$ space. Rather, they were concentrated in a curve representing the dispersion relation over the first Brillouin zone. The spectrum in Fig. 2(a) was calculated from a Fourier transform of particle velocities in time and space. (See Ref. [10] for details.) The data shown here are chosen only for the propagation direction that is parallel to one of the primitive lattice vectors, $\mathbf{k}\|\mathbf{a}$.

The naturally occurring modes satisfy dispersion relations [see Figs. 2(a) and 2(f)]. Our experiment was performed using a finite-size lattice. For wavelengths smaller than the crystal size, i.e., $k>0.1$ mm^{-1}, we can use the theoretical dispersion relation shown in Fig. 2(f). It was obtained by solving a linearized equation of motion in a triangular lattice with Yukawa interaction potentials [13]. The Yukawa potential is defined by $\phi_i=\Sigma_j Q_j \exp(-r_{ij}/\lambda_D)/4\pi\epsilon_0 r_{ij}$, where Q_j is the charge on particle j, r_{ij} is the distance between two particles, and λ_D is the shielding length.

From a best fit between the observed spectrum and the theoretical dispersion relation, Q and the shielding parameter $\kappa\equiv a/\lambda_D$ were estimated to be 16 000e and 1.2, respectively. Using the measured Q, κ, T, and a, we estimate that the Coulomb coupling parameter $\Gamma\equiv Q^2\exp(-\kappa)/4\pi\epsilon_0 a k_B T$ and $\omega_0\equiv(Q^2/4\pi\epsilon_0 m a^3)^{-1/2}$ had values 4000 and 13.6 s^{-1}, respectively. This large value of Γ confirms that the particles in our suspension were strongly coupled.

The spectrum width reflects damping of waves. For our

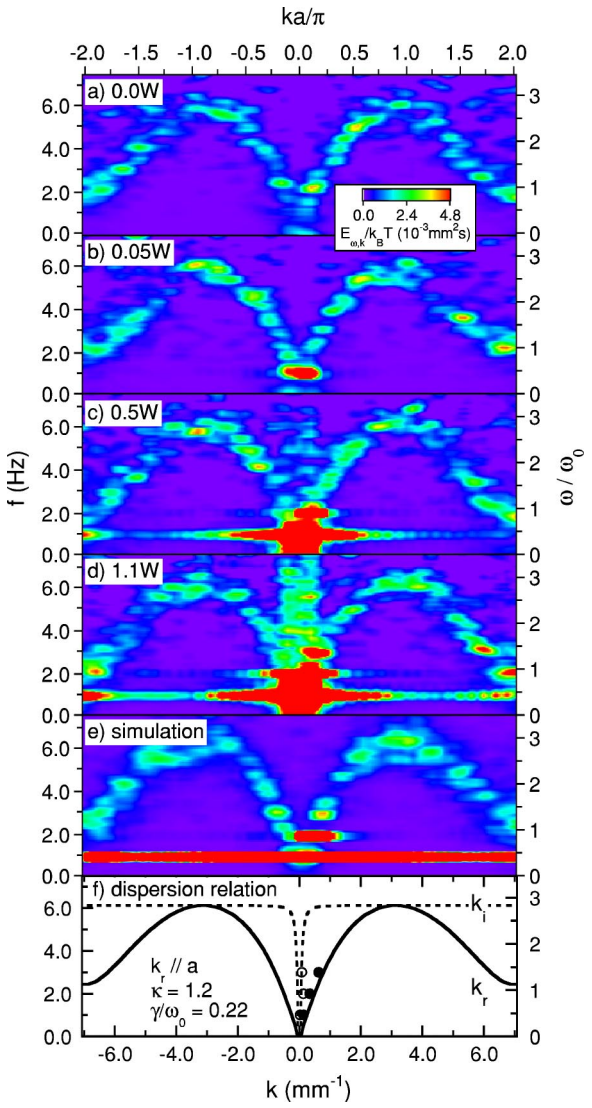

FIG. 2. (Color online) Wave spectra and a dispersion relation of longitudinal mode in a 2D plasma crystal. The wave propagation direction is parallel to one of the primitive lattice vectors, $\mathbf{k}\|\mathbf{a}$. Spectra are shown over the first Brillouin zone. (a)–(d) Experimental results for energy density maps in ω-$\mathbf{k}$ space. (a) Without intentional wave excitation, (b) with external wave excitation at $P=0.05$ W, (c) 0.5 W, and (d) 1.1 W. The bright color indicates high-energy concentration of waves. (e) Simulation result for an energy density map. (f) Theoretical dispersion relation. Solid and broken curves are k_r and k_i, respectively. Filled and open circles are k_r and k_i, experimentally obtained from the phase and amplitude fitting in Fig. 4.

Fourier analysis method, the frequency width is given by $\nu/4\pi$, where ν is the damping rate. The observed frequency width of the natural phonon spectrum was roughly 0.25 Hz. It corresponds to the values estimated from Epstein drag rate [21] so that in our system, particle motions were restricted by a gas friction.

IV. WAVE EXCITATION METHOD

To excite longitudinal waves in the lattice intentionally, we applied the radiation force of an argon laser, which was

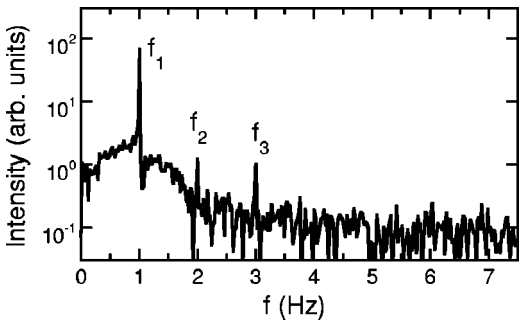

FIG. 3. Frequency spectrum of the intensity-modulated laser beam, i.e., the driving force for wave excitation. The higher harmonic components are approximately two order of magnitude smaller than the fundamental component.

incident on a local region of the lattice. As in other experiments [7,9,15,16,22], the momentum of the photons is transferred to the particle by applying a forward force to the particle in the direction of the laser beam. This force is proportional to the laser intensity. By applying a temporal modulation to the laser intensity, it is possible to excite sinusoidal waves. The waves were launched parallel to one of the primitive lattice vectors, $\mathbf{k}\|\mathbf{a}$.

In our experiment, the laser beam was shaped and modulated using two scanning mirrors, shown in Fig. 1. A wave form applied to mirror SM1 caused this mirror to block a portion of the laser beam, which varied with time, so that the laser intensity was nearly sinusoidal with time, with a frequency of 1 Hz. We chose this low frequency because it falls well within the dispersionless, i.e., acousticlike portion of the dispersion relation for longitudinal waves. The frequency spectrum of this laser modulation, as measured using a photodiode, is shown in Fig. 3.

To shape the laser beam, it was bounced from a second mirror SM2 which oscillated rapidly at 200 Hz, which is much higher than any frequency for lattice motion. Then, the laser sheet was injected into a plasma crystal at an incident angle of 10°, which pushes the particles mainly in the horizontal direction. The laser sheet was focused at the center of the crystal with a telescope. The intensity profile of the laser sheet was a Gaussian function, i.e., $\propto\exp(-x^2/l_{\mathrm{exc}}^2)$, where the wave excitation width l_{exc} was 2.0 mm. In our experimental apparatus, the x coordinate was defined as parallel to the wave propagation direction, which is also the direction of the laser radiation. The y coordinate was defined as perpendicular to the x axis, shown in Fig. 1. From the parameters of the wave form applied to mirror SM2, we calculated that the width of the laser sheet in the y direction was ≈ 25 mm, which is larger than the 18 mm viewing width but smaller than the lattice size.

Due to this finite size of the laser sheet in the y direction, the radiation pressure force had a profile that could induce a shear motion. Particles were pushed forward in the x direction, but with a magnitude that varied with y. This profile was most uniform in the central region, which is where we viewed with the camera. The shear region was outside the viewing area of the camera.

To search for nonlinear effects, we repeated our

experiment at various laser powers. Our lowest power was 0.05 W, while highest was 1.9 W, as measured in the vacuum chamber. For comparison, for the experimental measurement of the dispersion relation by Nunomura *et al.* [9] using the same apparatus, the laser power was 0.5 W.

V. EXPERIMENTAL RESULTS OF NONLINEAR WAVES

A. Classification of wave fields

Before considering our experimental results, it is useful to distinguish the ''near field'' and ''far field'' regions for wave excitation. The near field includes the excitation region where the laser intensity is nonzero. Particles oscillate in the near field in response to the temporal modulation of the laser beam. Some of this particle oscillation can couple into a propagating wave that exits the near field. Away from the near field the laser intensity is zero, and there is no external disturbance; this region is termed the far field. This distinction between the near and far fields can be found also in the literature for the antenna-coupling problem in the excitation of electromagnetic waves in a plasma [23].

The chief subject of this paper is a demonstration of nonlinear propagation of longitudinal waves in the far field. For this purpose, it is not necessary to fully measure and model all the phenomena in the near field. It is sufficient to characterize the longitudinal wave only in the far field region, beginning at the boundary with the near field. Here we define this boundary as approximately $x = l_{\mathrm{exc}}$, which is the location where the laser intensity is reduced by a factor $1/e$ as compared to its peak.

At the boundary of the near and far fields, particle velocity in the x direction is primarily a superposition of a strong sinusoidal disturbance at the fundamental of 1 Hz and a weaker sinusoidal disturbance at the second harmonic of 2 Hz. The presence of the second harmonic at this location arises from possibly two mechanisms; the laser intensity itself has some second harmonic, as shown in Fig. 3, and there may be harmonic generation in the near field region due to nonlinear particle oscillations. For our purposes in characterizing the particle motion in the far field, it does not matter exactly which mechanism in the near field produced the wave amplitudes at the boundary. It is sufficient to characterize the wave amplitudes beginning at the boundary and propagating outward into the far field, as we explain next.

B. Nonlinear wave interactions in a far field region

Spectra of the wave energy for longitudinal particle motion, i.e., for particle motion in the x direction, are shown in Fig. 2. At the lowest laser power of 0.05 W in Fig. 2(b), only the fundamental at 1 Hz can be identified, above the level of the naturally occurring waves that are presented in Fig. 2(a). As the laser power is increased to 0.5 W in Fig. 2(c), a second harmonic appears, and at a higher power of 1.1 W in Fig. 2(d), a third harmonic is present. These spectra were prepared by averaging the wave energy over the entire far field region viewed by the camera, 2 mm$<x<$16 mm. To more completely characterize the waves in the far field, it is necessary to report the spatial profiles of the wave amplitudes as a function of x, which we shall do next.

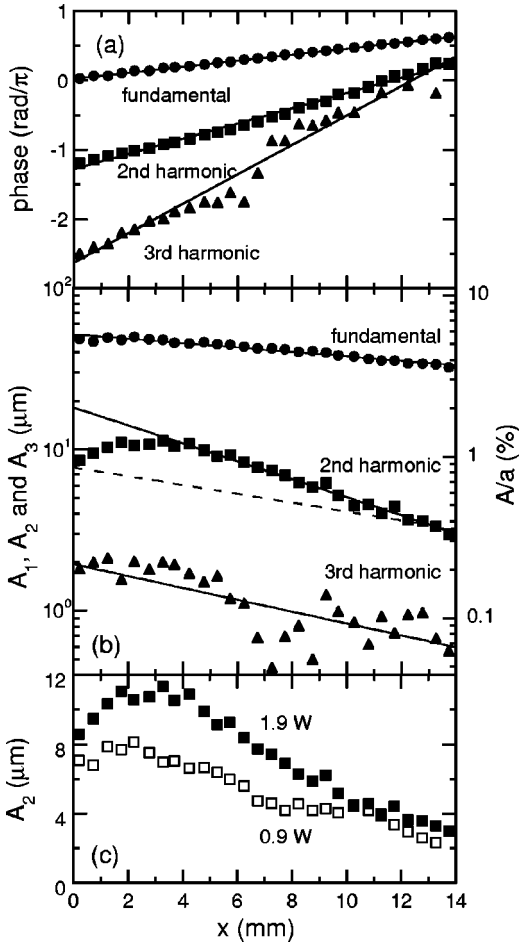

FIG. 4. (a) Phases and (b) amplitudes of the fundamental and the wave harmonics at $P = 1.8$ W. As a wave propagates, its phase increases linearly while its amplitude decreases exponentially, except for the second harmonic. The amplitude of the second harmonic initially increased with distance, then decreased, indicating nonlinear effects in the wave-wave interactions. The wave was excited at $x = 0$. (c) A_2 vs x in a linear scale, showing amplitude growth (0 mm$<x<$4 mm). For comparison, simple decay of A_2 at $P = 0.9$ W is shown, which is plotted by the open squares.

The amplitudes of each harmonic, i.e., the fundamental, second, and third harmonics, A_1, A_2, and A_3, respectively, as the waves propagate away from the near field, are shown in Fig. 4(b), for our highest laser power of 1.9 W. The data are shown in a semilogarithmic plot. The amplitude of the fundamental exhibits an exponential decay with distance x from the excitation region. The third harmonic similarly exhibits an exponential decay.

Our data also provide the phase of the waves, as shown in Fig. 4(a). The phase increases linearly with distance, as expected for the propagation of a sinusoidal wave, for all three modes. The fundamental mode has a wavelength of $2\pi/k_r = 45$ mm, as measured from the slope of the wave's phase. The second and third harmonics have a shorter wavelength. The corresponding real wave number k_r, as computed from the slopes in Fig. 4(a), is plotted as the solid data point in the linear dispersion relation of Fig. 2(f). The open datapoints in Fig. 2(f) are for the imaginary part of the wave number k_i,

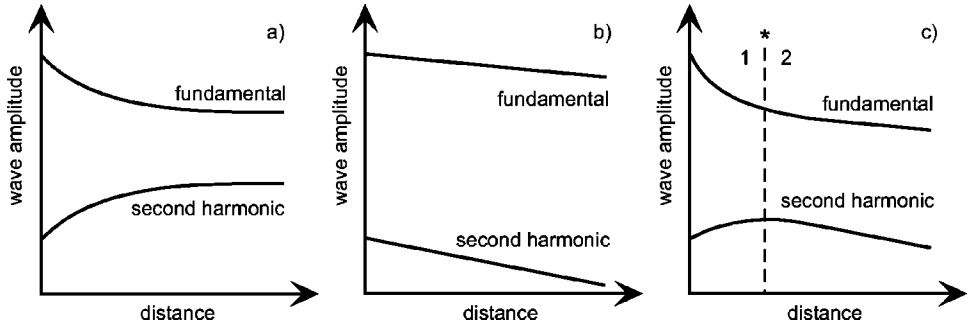

FIG. 5. Sketch showing the qualitative trends for wave amplitudes in far field, plotted vs distance from the excitation region. (a) *Nonlinear effect only, without damping*: Due to nonlinear wave-wave interactions, the amplitude of the fundamental decreases, and transfers its energy into the second wave harmonic, so that the second harmonic is amplified as it propagates. The amplification of second harmonic continues until the amplitude of fundamental becomes too small to couple any more energy to the second harmonic. (b) *Linear effect with damping*: A wave at a higher frequency is expected to damp more rapidly than at a low frequency, due to a gas friction, as predicted by the theoretical dispersion relation for linear waves. (c) *Nonlinear effect with damping*: For small distances (region 1), the amplitude of the fundamental is sufficient to provide nonlinear coupling into the second harmonic, so that the latter grows with distance, until it reaches a distance where the fundamental has been diminished considerably by damping. For larger distances (region 2), both waves are damped, as for linear waves.

as computed by fitting the experimental data in Fig. 4(b) to an exponential decay. The theoretical dispersion relation in Fig. 2(f) includes the imaginary part, shown as a dashed line, computed using an Epstein rate $\nu = 3.0\ \mathrm{s}^{-1}$, corresponding to our experimental gas pressure and particle size.

Our chief experimental result is that the spatial profile of the second harmonic exhibits an amplification of the wave at this frequency, as it propagates away from the excitation region. This amplification can be seen in Fig. 4(b) for distances roughly in the range $0\ \mathrm{mm} < x < 4\ \mathrm{mm}$. Note that the wave amplitude does not decrease exponentially with distance in this range as would be expected from the dispersion relation for linear waves; instead it increases approximately 20%. For comparison, a dashed line is drawn with a slope corresponding to the damping rate of the dispersion relation for a linear wave in an infinite lattice.

The amplification of the second harmonic as it propagates is observed only at a wave excitation with a high laser power. For an excitation with a lower laser power, the wave harmonics simply decay, shown by open squares in Fig. 4(c). Here, A_2 is plotted with a linear scale to show two different types of spatial profiles more clearly.

C. Discussion for amplification of harmonics

The augmentation of the second harmonic wave energy, in comparison to the damping that would be expected for a purely linear wave propagation, is our primary experimental indication of nonlinear wave-wave interaction. To explain why this is due to nonlinear effects, we begin by making an analogy to the theory of nonlinear optics.

A simple model, without damping, yields a description of how the amplitudes of the fundamental and the harmonics vary with distance, as in Eq. (4.20) of Ref. [24]. Beginning with a wave at the fundamental and a weaker wave at the second harmonic, as both waves propagate in the same direction, energy is transferred between the waves by nonlinear interactions in the medium through which they propagate. The amplitude of the second harmonic increases with distance by taking energy from the fundamental, and the amplitude of the fundamental correspondingly diminishes. The rate of the amplification of the second harmonic is proportional to the square of the amplitude of the fundamental. These qualitative trends are sketched in Fig. 5(a).

Another case to consider is that of linear waves in the presence of damping. In this case, waves undergo only a decrease in amplitude with respect to propagation distance. This is sketched qualitatively in Fig. 5(b).

Our experimental results can be explained as a combination of the two effects described above. First, we consider propagation at small distances, as sketched in part 1 of Fig. 5(c). The amplitude of the fundamental is large, so that its square is particularly large and there is significant transfer of wave energy from the fundamental to the second harmonic via nonlinear effects. As the fundamental wave propagates, its amplitude diminishes, not only due to the transfer of energy to the second harmonic but also due to the damping. Next, we consider propagation at larger distances from the excitation region, as sketched in part 2 of Fig. 5(c). At a sufficiently large distance, the amplitude of the fundamental becomes so small that the rate of transfer of energy to the second harmonic is less than the damping of the second harmonic. Beyond this point, marked with an asterisk * in Fig. 5(c), the amplitude of the second harmonic diminishes with distance.

D. Discussion for nonlinear phenomena in a near field region

While the results in the far field, presented above, are our primary results, we also discuss some of the phenomena that take place in the near field region, where the laser intensity is significant. The incident laser power pushes particles in the near field. There are several channels into which this energy can flow. First, energy can be dissipated by damping of particle motion, within the excitation region, by gas friction. Second, some of the wave energy is transferred directly into the longitudinal wave at the same frequency. Third, because the laser beam profile has a shear, some of the wave is also

transferred to the transverse wave, as in Ref. [8], which we did not attempt to measure here. Fourth, some of the wave energy is transferred into the sloshing mode, as was demonstrated previously in Ref. [9]. Finally, at large amplitudes, some of the incident wave energy can flow into one of the several nonlinear mechanisms.

There are at least two nonlinear mechanisms in the near-field region: nonlinear oscillations and plastic deformation. Nonlinear oscillations in the near-field region generate, for example, additional energy in the second harmonic from the pump at the fundamental; this kind of harmonic generation does not necessarily require any wave propagation if it occurs inside the near-field region where the laser radiation force is significant. Plastic deformation, i.e., breaking of bonds, can occur due to shear in the particle velocity. If there is plastic deformation, then the lattice has some liquid-like properties in some local region of the particle suspension. The particle suspension may therefore be able to sustain a vortex motion, which is an additional outlet for the energy from the laser.

We believe that at our highest laser powers, there was some plastic deformation outside the viewing area of our camera, because we observed a constant drift of particles in the $+x$ direction (the particle drift velocity is ≈ 0.1 mm/s), which can only be explained if there is a circulation of particles out of the observed region. This circulation must be closed by a vortex on either side of the viewing region, so that particles ultimately flow back into the viewing region. Within our viewing region there were very few defects, so that the lattice was crystalline, but our observation of circulation indicates that elsewhere there must have been some bond breaking or plastic deformation.

We are not able to quantitatitatively model all of these effects in the near field for our experiment. For the purpose of observing the wave propagation in the far field, they actually do not matter much. Regardless of the mechanisms that determine the exact amplitude of the waves at each frequency as they exit the near field, we can measure their amplitudes as they propagate through the far field to arrive out at our main results, presented earlier.

VI. NONLINEAR WAVE THEORY

Here, we introduce a nonlinear wave theory to discuss more about the harmonic generation mechanism in a far-field region. Our model system is a 2D triangular Yukawa crystal confined by an externally provided force. When we suppose that a wave is excited by a localized external perturbation and gradually damped due to a gas friction, the equation of a particle motion can be written as

$$\ddot{\mathbf{r}}_i + \nu \dot{\mathbf{r}}_i = (\mathbf{f}_{\text{Yukawa}} + \mathbf{f}_{\text{exc}} + \mathbf{f}_{\text{conf}})/m, \tag{1}$$

where $\mathbf{r}_i$ is the position of the ith particle and the overdots denote time derivatives. The particle interactions, i.e, repulsive Yukawa forces, are given by $\mathbf{f}_{\text{Yukawa}} = -Q_i \nabla \phi_i$. To model the experimental configuration, the forces for the wave excitation and the particle confinement are assumed to be $\mathbf{f}_{\text{exc}} = \mathbf{f}_{\text{exc0}} \exp(-(x/l_{\text{exc}})^2)(1-\cos \omega t)$ and $\mathbf{f}_{\text{conf}}/m = -\Omega^2 \mathbf{r}_i$, respectively. Here, Ω is the eigenfrequency of the sloshing mode, $\mathbf{r}_i = \mathbf{r}_i^0 + \mathbf{u}$, $\mathbf{r}_i$ is the equilibrium position of particles, and $\mathbf{u}$ is the particle displacement from their equilibrium.

If $u/a \ll 1$ (as typical in experiments, A_1/a is typically several percent), Eq. (1) can be expanded with respect to u as follows:

$$\ddot{u} + \nu \dot{u} = Du + C_s^2 \partial_x ((\Lambda_2/2)(\partial_x u)^2 + (\Lambda_4/3)(\partial_x u)^3) + (f_{\text{exc}} + f_{\text{conf}})/m. \tag{2}$$

On the right-hand side (RHS), Du represents the linear response of Yukawa interactions with respect to u, i.e., D is a dynamical matrix (in Ref. [11]). The second and third terms represent the second and the third order nonlinear terms, respectively. Here, C_s is the sound speed and $\Lambda_{2,4}$ are nonlinearity coefficients defined in Ref. [18]. These coefficients depend on the wave propagation direction and κ. In our experimental condition, Λ_2 and Λ_4 are -3.37 and 0.49, respectively, for $\kappa \approx 1$. When we consider only the first term Du in the RHS of Eq. (2), the solution for sinusoidal oscillation gives the dispersion relation, which is the same as plotted in Fig. 2(f) for our experimental conditions.

In order to solve Eq. (2), we assume that all forces are small. Using the expansion parameter ϵ and writing the order of f as ϵ, u can be represented as follows:

$$u = U_0(x) + U_1(x)\exp(i\omega t + \text{c.c.}) + U_2(x)\exp(2i\omega t + \text{c.c.}) + \cdots. \tag{3}$$

Here, $U_0 \sim \epsilon$, $U_1 \sim \epsilon$, and $U_2 \sim \epsilon^2$ are the spatial distributions for the zero, fundamental, and second harmonics. Equating terms with the same harmonic number and re-expanding further with respect to ϵ, one can finally find the following solutions for the Fourier amplitudes of wave harmonics:

$$U_{0k} = G_{0,k} F_k^{(0)}/m, \tag{4a}$$

$$U_{1k} = -1/2 G_{\omega,k} F_k^{(0)}/m, \tag{4b}$$

$$U_{2k} = 1/2 i C_s^2 \Lambda_2 G_{2\omega,k} \int dk' k k' (k'-k) U_{1k'} U_{1,(k-k')}, \tag{4c}$$

$$U_{3k} = C_s^2 G_{3\omega,k} \Big(1/2 i \Lambda_2 \int dk' k k' (k'-k) U_{1k'} U_{2,(k-k')} + 1/3 \Lambda_4 \int dk' dk'' k k' k'' (k-k'-k'') \times U_{1k'} U_{1k''} U_{1,(k-k'-k'')} \Big). \tag{4d}$$

Here, the function $G_{\omega,k}$ is given by

$$G_{\omega,k} = [\omega_k^2 + \Omega^2 - \omega(\omega - i\nu)]^{-1}. \tag{5}$$

Looking at Eqs. (4c) and (4d), one notices that the generation of higher harmonics comes from products of the wave amplitudes, i.e., nonlinear terms. For example, the second harmonics is generated by two-wave coupling of the fundamental mode. The third harmonic is generated by either two-wave coupling between the fundamental and the second harmonic (first term), or three-wave coupling among the fundamental harmonics (second term). To summarize, the amplitude of the nth harmonic is proportional to the nth power of the amplitude of the fundamental mode.

VII. MD SIMULATION

We also performed a MD simulation to reproduce the generation of wave harmonics as observed in the experiments. By numerically solving the equations of motion, Eq. (1), using the experimentally determined values of Q, m, a, ν, all particle orbits were computed for several seconds.

Our simulation procedure is as follows. First, 721 particles were dispersed randomly in a 2D simulation area. Their equilibrium positions were computed, taking into account the external confining force, choosing $\Omega = 2.3\ \mathrm{s}^{-1}$ in Eq. (1) to achieve the same κ as in the experiment. For this particular confinement strength and the particle number introduced in the system, crystal size was ≈ 3 cm in diameter. Then, to imitate the random particle motion, the random force that has a spectrum of uniform amplitude in the frequency space was applied to each particle. We adjusted the random force amplitude to have approximately the same T as in the experiment. After these processes, we excited a wave by applying a localized force as in Eq. (1), where l_{exc} was chosen to be 2.0 mm to match the experiment.

An example of a wave spectrum from the MD simulation is shown in Fig. 2(e), which is qualitatively similar to the experimental spectra. As expected, the second and weak third harmonics were detected at a large amplitude of the fundamental wave excitation. In addition, the naturally occurring modes, associated with the random particle motions, were also reproduced and satisfied the dispersion relation.

VIII. SUMMARY

We observed the generation of longitudinal wave harmonics in a 2D plasma crystal. The wave harmonics were generated only when the fundamental mode had a sufficiently large amplitude. The second harmonic was amplified for a short distance as it propagates, then it was damped by a gas friction. A MD simulation for a nonlinear wave was performed, and its wave spectrum agreed qualitatively with experimental results. The nonlinear wave theory was presented and nonlinear wave-wave interactions were discussed.

ACKNOWLEDGMENTS

We thank K. Avinash, R. Quinn, D. Samsonov, A. Ivlev, and S. Matsukiyo for useful discussions. S.N. acknowledges the Japan Society of the Promotion of Science. Experiments were performed at The University of Iowa, funded by NASA and the U.S. Department of Energy.

[1] For example, R.Z. Sagdeev and Galeev, *Nonlinear Plasma Theory* (W.A. Benjamin, New York, 1969); J. Weiland and H. Wilhelmsson, *Coherent Non-Linear Interaction of Waves in Plasmas* (Pergamon Press, Oxford, 1977).
[2] U. Konopka, G.E. Morfill, and L. Ratke, Phys. Rev. Lett. **84**, 891 (2000).
[3] J.H. Chu and Lin I, Phys. Rev. Lett. **72**, 4009 (1994).
[4] H. Thomas, G.E. Morfill, V. Demmel, J. Goree, B. Feuerbacher, and D. Mohlmann, Phys. Rev. Lett. **73**, 652 (1994).
[5] Y. Hayashi and K. Tachibana, Jpn. J. Appl. Phys., Part 1 **33**, L804 (1994).
[6] J.B. Pieper and J. Goree, Phys. Rev. Lett. **77**, 3137 (1996).
[7] A. Homann, A. Melzer, R. Madani, and A. Piel, Phys. Lett. A **242**, 173 (1998).
[8] S. Nunomura, D. Samsonov, and J. Goree, Phys. Rev. Lett. **84**, 5141 (2000).
[9] S. Nunomura, J. Goree, S. Hu, X. Wang, and A. Bhattacharjee, Phys. Rev. E **65**, 066402 (2002).
[10] S. Nunomura, J. Goree, S. Hu, X. Wang, A. Bhattacharjee, and K. Avinash, Phys. Rev. Lett. **89**, 035001 (2002).
[11] F.M. Peeters and X. Wu, Phys. Rev. A **35**, 3109 (1987).
[12] D.H.E. Dubin, Phys. Plasmas **7**, 3895 (2000).
[13] X. Wang, A. Bhattacharjee, and S. Hu, Phys. Rev. Lett. **86**, 2569 (2001).
[14] D. Samsonov, A.V. Ivlev, R.A. Quinn, G. Morfill, and S. Zhdanov, Phys. Rev. Lett. **88**, 095004 (2002).
[15] V. Nosenko, S. Nunomura, and J. Goree, Phys. Rev. Lett. **88**, 215002 (2002).
[16] A. Melzer, S. Nunomura, D. Samsonov, Z.W. Ma, and J. Goree, Phys. Rev. E **62**, 4162 (2000).
[17] F. Melandsø, Phys. Plasmas **3**, 3890 (1996).
[18] S.K. Zhdanov, D. Samsonov, and G.E. Morfill, Phys. Rev. E **66**, 026411 (2002).
[19] D. Samsonov, J. Goree, H.M. Thomas, and G.E. Morfill, Phys. Rev. E **61**, 5557 (2000).
[20] R.A. Quinn and J. Goree, Phys. Rev. E **61**, 3033 (2000).
[21] P. Epstein, Phys. Rev. **23**, 710 (1924).
[22] B. Liu, V. Nosenko, J. Goree, and L. Boufendi, Phys. Plasmas **10**, 9 (2003).
[23] For example, F. Skiff, M. Ono, and P. Colestock, Phys. Fluids **28**, 2453 (1985).
[24] D.L. Mills, *Nonlinear Optics* (Springer, Berlin, 1991).